

Article

# A Meshless Method Based on the Laplace Transform for the 2D Multi-Term Time Fractional Partial Integro-Differential Equation

Kamran <sup>1</sup>, Zahir Shah <sup>2</sup>  and Poom Kumam <sup>3,4\*</sup> and Nasser Aedh Alreshidi <sup>5</sup> 

<sup>1</sup> Department of Mathematics, Islamia College Peshawar, Peshawar 25000, Khyber Pakhtoon Khwa, Pakistan; kamran.maths@icp.edu.pk

<sup>2</sup> Department of Mathematics, University of Lakki Marwat, Lakki Marwat 28420, Khyber Pakhtunkhwa, Pakistan; zahir@ulm.edu.pk

<sup>3</sup> KMUTT Fixed Point Research Laboratory, Room SCL 802 Fixed Point Laboratory, Science Laboratory Building, Department of Mathematics, Faculty of Science, King Mongkut's University of Technology Thonburi (KMUTT), 126 Pracha-Uthit Road, Bang Mod, Thung Khru, Bangkok 10140, Thailand

<sup>4</sup> Department of Medical Research, China Medical University Hospital, China Medical University, Taichung 40402, Taiwan

<sup>5</sup> College of Science Department of Mathematics, Northern Border University, Arar 73222, Saudi Arabia; nasser.alreshidi@nbu.edu.sa

\* Correspondence: poom.kum@kmutt.ac.th

Received: 8 October 2020; Accepted: 3 November 2020; Published: 6 November 2020



**Abstract:** In this article, we propose a localized transform based meshless method for approximating the solution of the 2D multi-term partial integro-differential equation involving the time fractional derivative in Caputo's sense with a weakly singular kernel. The purpose of coupling the localized meshless method with the Laplace transform is to avoid the time stepping procedure by eliminating the time variable. Then, we utilize the local meshless method for spatial discretization. The solution of the original problem is obtained as a contour integral in the complex plane. In the literature, numerous contours are available; in our work, we will use the recently introduced improved Talbot contour. We approximate the contour integral using the midpoint rule. The bounds of stability for the differentiation matrix of the scheme are derived, and the convergence is discussed. The accuracy, efficiency, and stability of the scheme are validated by numerical experiments.

**Keywords:** fractional partial integro differential; weakly singular kernel; Laplace transform; local meshless method; contour integration; Talbot's contour; midpoint rule

## 1. Introduction

Recently, the theory fractional calculus has gained significant attention in the field of engineering and other sciences because of its various applications in modeling numerous phenomena. For example numerous phenomena in the mathematical biology, physics, and engineering fields can be described by fractional integro-differential equations (FIDEs), fractional partial integro-differential equations (FPIDEs), and fractional partial differential equations (FPDEs). In particular, several phenomena give rise to fractional partial integro-differential equations such as viscoelastic phenomena, signal processing, and fluid mechanics (see [1–4] and the references therein).

Finding exact or numerical solutions of FPIDEs with weakly singular kernels is an important task. Due to the possible singularities of the kernel function at the origin [5], sharp changes will occur in the solution, so the exact/analytic solution may be difficult to obtain [6]. Therefore, the alternate way is to develop an accurate numerical scheme. The approximation of FPIDEs and partial integro-differential equations (PIDEs) has been considered by many researchers, such as the authors in [7–10], who used the

finite difference (FDM) and finite element (FEM) methods for the approximation of PIDEs. The authors in [11,12] used spline collocation methods for approximating PIDEs of the parabolic and hyperbolic type, respectively. Huang [13] solved parabolic PIDEs using the time discretization scheme. In [3], the B-spline solution of FPIDEs was found. The authors in [4] used the reproducing kernel method for the approximation of FPIDEs. A backward Euler difference scheme was constructed for the approximation of the partial integro-differential equation with multi-term kernels [14]. Other valuable work on integro-differential equations can be found in [15–26] and the references therein. Recently, the meshless methods have attracted researchers and become the primary tool for interpolating multidimensional scattered data.

In the literature, we can find a large number of meshless methods developed for the numerical treatment of different PDEs or PIDEs such as the authors in [27], who proposed the RBF-FD method for the approximation of PIDEs. In [28], a local method was developed for the approximation of PIDEs. In [29], the nonlinear PIDEs were approximated via the RBF and theta method. Similarly, the authors in [30] proposed a local method with the optimal shape parameter for PIDEs.

In this article, the Laplace transform and localized meshless method are combined for the approximation of the solution of FPIDEs with a weakly singular kernel. In the literature, we can find some valuable work on the Laplace transform coupled with other methods in [31–39] and the references therein. We consider an FPIDE of the form [40]:

$$\sum_{\rho=1}^m d_{\rho} D_{\tau}^{\gamma_{\rho}} U(\zeta, \tau) - \mathfrak{S}^{(\alpha)} \mathcal{L}U(\zeta, \tau) = f(\zeta, \tau), \zeta \in \Omega, \text{ and } \tau \in [0, T], \tag{1}$$

subject to the initial and boundary conditions:

$$\begin{aligned} U(\zeta, 0) &= \Theta(\zeta), \zeta \in \Omega, \\ \mathcal{B}U(\zeta, \tau) &= h(\zeta, \tau), \zeta \in \partial\Omega, \tau \in [0, T]. \end{aligned} \tag{2}$$

where  $0 < \gamma_1 \leq \gamma_2 \leq \dots \leq \gamma_m \leq 1$ ,  $d_{\rho} > 0$ ,  $m \in \mathbb{N}$ ,  $\Omega = [0, L]^2$ ,  $\Theta$  is a given function,  $\mathcal{L} = \Delta$ , and  $\mathcal{B}$  is the boundary operators.  $D_{\tau}^{\gamma}$  is the Caputo derivative of order  $\gamma$  defined as [41,42]:

$$D_{\tau}^{\gamma} U(\tau) = \frac{1}{\Gamma(p - \gamma)} \int_0^{\tau} (\tau - \theta)^{p - \gamma - 1} \frac{d^p}{d\theta^p} U(\theta) d\theta, \quad p - 1 \leq \gamma \leq p, \quad p \in \mathbb{N}; \tag{3}$$

in particular for  $p = 1$ , we have:

$$D_{\tau}^{\gamma} U(\tau) = \frac{1}{\Gamma(1 - \gamma)} \int_0^{\tau} (\tau - \theta)^{-\gamma} \frac{d}{d\theta} U(\theta) d\theta, \quad 0 \leq \gamma \leq 1, \tag{4}$$

and the  $\alpha$ th integral  $\mathfrak{S}^{(\alpha)} U(\tau)$  is defined as [42]:

$$\mathfrak{S}^{(\alpha)} U(\tau) = \frac{1}{\Gamma(\alpha)} \int_0^{\tau} (\tau - \theta)^{\alpha - 1} U(\theta) d\theta. \tag{5}$$

The Laplace transform of  $U(\tau)$  is defined by:

$$\widehat{U}(s) = \mathcal{L}\{U(\tau)\} = \int_0^{\infty} e^{-s\tau} U(\tau) d\tau, \tag{6}$$

and the Laplace transform of  $D_{\tau}^{\gamma}$  is given by:

$$\mathcal{L}\{D_{\tau}^{\gamma} U(\tau)\} = s^{\gamma} \widehat{U}(s) - \sum_{i=0}^{m-1} s^{\gamma - i - 1} U^{(i)}(0), \tag{7}$$

while the Laplace transform of  $\mathfrak{S}^{(\alpha)}U(\tau)$  is given by:

$$\mathcal{L}\{\mathfrak{S}^{(\alpha)}U(\tau)\} = \frac{1}{\Gamma(\alpha)} \left( \frac{\Gamma(\alpha)\widehat{U}(s)}{s^\alpha} \right). \tag{8}$$

Equation (1) involves multi-term time fractional derivatives, which are helpful in modeling complex physical systems such as the physical multi-rate phenomenon [43], fractional Zener model [44], heavily damped motion, Newtonian fluid [42,45], and anomalous relaxation process [46]. The integral term represents the viscosity part of Equation (1) [40]. Equation (1) can be obtained from the partial integro-differential equation:

$$\frac{\partial U(\zeta, \tau)}{\partial \tau} - \mathfrak{S}^{(\alpha)}\mathcal{L}U(\zeta, \tau) = f(\zeta, \tau), \quad \zeta \in \Omega, \tau \in [0, T],$$

by replacing the first order time derivative by a linear combination of fractional derivatives of different orders [47]. For  $m = 1$ , Equation (1) becomes the single term FPIDE of the form:

$$d_1 D_\tau^{\gamma_1} U(\zeta, \tau) - \mathfrak{S}^{(\alpha)}\mathcal{L}U(\zeta, \tau) = f(\zeta, \tau), \quad \zeta \in \Omega, \tau \in [0, T],$$

and for  $\alpha = 1$ , Equation (1) becomes the fractional multi-term diffusion equation:

$$\sum_{\rho=1}^m d_\rho D_\tau^{\gamma_\rho} U(\zeta, \tau) - \mathcal{L}U(\zeta, \tau) = f(\zeta, \tau), \quad \zeta \in \Omega, \tau \in [0, T].$$

## 2. Proposed Numerical Scheme

Taking the Laplace transform of Equations (1) and (2), we have:

$$d_1 s^{\gamma_1} \widehat{U}(\zeta, s) - d_1 s^{\gamma_1-1} \Theta(\zeta) + d_2 s^{\gamma_2} \widehat{U}(\zeta, s) - d_2 s^{\gamma_2-1} \Theta(\zeta) + \dots + d_m s^{\gamma_m} \widehat{U}(\zeta, s) - d_m s^{\gamma_m-1} \Theta(\zeta) - s^{-\alpha} \mathcal{L}\widehat{U}(\zeta, s) = \widehat{f}(\zeta, s), \tag{9}$$

$$\mathcal{B}\{\widehat{U}(\zeta, s)\} = \widehat{h}(\zeta, s); \tag{10}$$

combining the like terms, we obtain the following system:

$$(d_1 s^{\gamma_1} I + d_2 s^{\gamma_2} I + \dots + d_m s^{\gamma_m} I - s^{-\alpha} \mathcal{L}) \widehat{U}(\zeta, s) = \widehat{g}(\zeta, s), \tag{11}$$

$$\mathcal{B}\{\widehat{U}(\zeta, s)\} = \widehat{h}(\zeta, s), \tag{12}$$

where:

$$\widehat{g}(\zeta, s) = d_1 s^{\gamma_1-1} \Theta(\zeta) + d_2 s^{\gamma_2-1} \Theta(\zeta) + \dots + d_m s^{\gamma_m-1} \Theta(\zeta) + \widehat{f}(\zeta, s),$$

where  $I$  is the identity operator and  $\mathcal{L}$  and  $\mathcal{B}$  are the governing and the boundary differential operators. In order to solve the system given in (11) and (12), first, we employ the local meshless method to discretize the operators  $\mathcal{L}$  and  $\mathcal{B}$ . When we are done with the discretization of these two operators, the system of Equations (11) and (12) is solved in parallel for each point  $s$  along some suitable path  $\Gamma$  in the complex plane ( see, e.g., [16,34]). Finally, the solution of the original problem (1) and (2) is obtained using the inverse Laplace transform. The local meshless method for the discretization of the given differential operators  $\mathcal{L}$  and  $\mathcal{B}$  is described in the next section.

### 2.1. Localized Meshless Method

In the localized meshless method for a given set of nodes  $\{\zeta_i\}_{i=1}^N \subset \Omega$ , the local meshless approximate of the function  $\widehat{U}(\zeta)$  has the form [48]:

$$\widehat{U}(\zeta_i) = \sum_{\zeta_h \in \Omega_i} \lambda_h^i \phi(\|\zeta_i - \zeta_h\|), \tag{13}$$

where  $\phi(r)$  is a radial kernel,  $r = \|\zeta_i - \zeta_h\|$  is the distance between  $\zeta_i$  and  $\zeta_h$ ,  $\lambda^i = \{\lambda_h^i\}_{h=1}^n$  is the vector of expansion coefficients,  $\Omega$  is the global domain, and  $\Omega_i$  is a local domain containing  $\zeta_i$ , and  $n$  nodes around it. Hence, we obtain  $N$  linear systems of order  $n \times n$  given by:

$$\widehat{U}^i = \Phi^i \lambda^i, i = 1, 2, 3, \dots, N; \tag{14}$$

the elements of the system matrix  $\Phi^i$  are  $b_{ij}^i = \phi(\|\zeta_i - \zeta_h\|)$ , where  $\zeta_i, \zeta_h \in \Omega_i$ , and the unknowns  $\lambda^i = \{\lambda_h^i\}_{h=1}^n$  are found by solving each  $n \times n$  system. Next, the operator  $\mathcal{L}\widehat{U}(\zeta)$  is approximated by:

$$\mathcal{L}\widehat{U}(\zeta_i) = \sum_{\zeta_h \in \Omega_i} \lambda_h^i \mathcal{L}\phi(\|\zeta_i - \zeta_h\|). \tag{15}$$

The above Equation (15) can be expressed as:

$$\mathcal{L}\widehat{U}(\zeta_i) = \lambda^i \cdot \mathbf{v}^i, \tag{16}$$

where  $\lambda^i$  is an  $n$ -column vector and  $\mathbf{v}^i$  is an  $n$ -row vector with entries:

$$\mathbf{v}^i = \mathcal{L}\phi(\|\zeta_i - \zeta_h\|), \zeta_h \in \Omega_i; \tag{17}$$

solving Equation (14), for  $\lambda^i$ , we have,

$$\lambda^i = (\Phi^i)^{-1} \widehat{U}^i. \tag{18}$$

From Equation (18), we use  $\lambda^i$  in Equation (16) and get,

$$\mathcal{L}\widehat{U}(\zeta_i) = \mathbf{v}^i (\Phi^i)^{-1} \widehat{U}^i = \mathbf{w}^i \widehat{U}^i, \tag{19}$$

where,

$$\mathbf{w}^i = \mathbf{v}^i (\Phi^i)^{-1}. \tag{20}$$

Thus, the local meshless approximation for the differential operator  $\mathcal{L}$  at each center  $\zeta_i$  is given as:

$$\mathcal{L}\widehat{U} \equiv \mathbf{D}\widehat{U}. \tag{21}$$

The differentiation matrix  $\mathbf{D}$  is sparse and has order  $N \times N$  containing  $n$  number of non-zero entries, where  $n \in \Omega_i$ . The matrix  $\mathbf{D}$  approximates the linear differential operator  $\mathcal{L}$ . The approximation for the boundary differential operator  $\mathcal{B}$  can be done in the same way.

### 3. Numerical Inversion of the Laplace Transform

Following the discretization by the local meshless method of the linear differential and boundary operators  $\mathcal{L}$  and  $\mathcal{B}$ , respectively, the system (11) and (12) is solved in parallel for each point  $s$  along some suitably chosen path in the complex plane. Finally, we get the solution of the problem (1) and (2) using the inversion formula:

$$U(\zeta, \tau) = \frac{1}{2\pi i} \int_{\sigma - i\infty}^{\sigma + i\infty} e^{s\tau} \widehat{U}(\zeta, s) ds = \frac{1}{2\pi i} \int_{\Gamma} e^{s\tau} \widehat{U}(\zeta, s) ds, \sigma > \sigma_0, \tag{22}$$

where  $\sigma_0 \in \mathbb{R}$  is called the converging abscissa and  $\Gamma$  is an initially appropriately chosen line connecting  $\sigma - i\infty$  to  $\sigma + i\infty$ . This means all the singularities of  $\widehat{U}(\zeta, s)$  lie in the half plane  $\text{Re}s < \sigma$ . The approximation of the integral (22) is hard because of the slow decaying transform  $\widehat{U}(\zeta, s)$  and the

highly oscillatory exponential factor  $e^{s\tau}$ . To handle these issues, we use the strategy suggested by Talbot [49]. He suggested the deformation of the contour of integration  $\Gamma$ . In particular, he suggested that the contour  $\Gamma$  be deformed in such a way that its real part starts and ends in the left half plane, and it encloses all the singularities of the transform  $\widehat{U}(\zeta, s)$ . Cauchy’s theorem allows such a deformation provided that  $\widehat{U}(\zeta, s)$  has no singularities on the contour [49]. On such contours, the exponential factor decays rapidly, which makes the integral in Equation (22) suitable for approximation using the midpoint or trapezoidal rule [49–51]. We consider a Hankel contour with the parametric form given by [50]:

$$\Gamma : s = s(\vartheta), \quad -\pi \leq \vartheta \leq \pi, \tag{23}$$

where  $Res(\pm\pi) = -\infty$ , and  $s(\vartheta)$  is defined as:

$$s(\vartheta) = \frac{M}{\tau}\theta(\vartheta), \quad \theta(\vartheta) = -\sigma + \mu\vartheta \cot(\gamma\vartheta) + \nu i\vartheta, \tag{24}$$

where the parameters  $\sigma$ ,  $\gamma$ ,  $\mu$ , and  $\nu$  are to be described by the user. From Equations (22) and (24), we have:

$$U(\zeta, \tau) = \frac{1}{2\pi i} \int_{\Gamma} e^{s\tau} \widehat{U}(\zeta, s) ds = \frac{1}{2\pi i} \int_{-\pi}^{\pi} e^{s(\vartheta)\tau} \widehat{U}(\zeta, s(\vartheta)) s'(\vartheta) d\vartheta. \tag{25}$$

We use the  $M$ -panel midpoint rule with uniform spacing  $k = \frac{2\pi}{M}$  to approximate the integral in Equation (25) as:

$$U_k(\zeta, \tau) = \frac{1}{Mi} \sum_{j=1}^M e^{s_j\tau} \widehat{U}(\zeta, s_j) \xi_j, \tag{26}$$

for  $\vartheta_j = -\pi + (j - \frac{1}{2})k$ ,  $s_j = s(\vartheta_j)$ ,  $s'_j = s'(\vartheta_j)$ .

#### 4. Convergence and Accuracy

In order to approximate the solution of FPIDEs using our proposed numerical scheme, the Laplace transform and local meshless method are used. In our numerical scheme, we employ the Laplace transform to the time dependent equation, which eliminates the time variable, and this process causes no error. Then, the local meshless method is utilized for approximating the time independent equation. The error estimate for local meshless method is of order  $O(\eta^{\frac{1}{\epsilon h}})$ ;  $0 < \eta < 1$ ;  $\epsilon$  is the shape parameter; and  $h$  is the fill distance [52]. In the process of approximating the integral in Equation (25), we achieve the convergence at different rates depending on the path  $\Gamma$ . While approximating the integral in Equation (25), the convergence order relies on the step  $k$  of the quadrature rule and the time domain  $[t_0, T]$  for  $\Gamma$ . In order to achieve high accuracy, we need to search for the most favorable values of the parameters involved in Equation (24). The authors [50] obtained the most suitable values of the parameters given as:

$$\sigma = 0.6122, \quad \mu = 0.5017, \quad \nu = 0.2645, \quad \text{and} \quad \gamma = 0.6407,$$

with the corresponding error estimate as:

$$\text{Error Estimate} = |U(\zeta, \tau) - U_k(\zeta, \tau)| = O(e^{-1.358M}).$$

The optimal contour is supposed to pass neither too close to nor too far from the singularities, in which case  $e^{s\tau}$  becomes too large. Moreover, to achieve the desired accuracy, the quadrature points are required to extend far enough into the left half plane. However, their contributions must not be less than the required accuracy.

The necessary steps of our method are presented in the following Algorithm 1.

---

**Algorithm 1:**

---

- 1: **Input:** The computational domain, the fractional order derivative in  $[0,1]$ , the final time, the contour of integration, the initial shape parameter and the other parameter of the given model, the inhomogeneous function, and other conditions.
  - 2: **Step 1:** Apply the Laplace transform to the problem (1) and (2), and obtain the time independent problem (11) and (12).
  - 3: **Step 2:** Discretize the linear differential operator  $\mathcal{L}$  and boundary operator  $\mathcal{B}$  using (21).
  - 4: **Step 3:** Solve the system of Equations (11) and (12) in parallel for each point  $s$  along the contour of integration  $\Gamma$  given in (18).
  - 5: **Step 4:** Compute the approximate solution using (25).
  - 6: **Output:** The approximate solution is  $U_k(\zeta, \tau)$ .
- 

**5. Stability Analysis**

In order to investigate the system (11) and (12) stability, we represent the system in discrete form as:

$$Y\hat{U} = \mathbf{b}, \tag{27}$$

where  $Y_{N \times N}$  is the sparse differentiation matrix obtained using the local meshless method described in Section 2.1. For the system (27), the constant of stability is given by:

$$C = \sup_{\hat{U} \neq 0} \frac{\|\hat{U}\|}{\|Y\hat{U}\|}, \tag{28}$$

where the constant  $C$  is finite for any discrete norm  $\|\cdot\|$  defined on  $R^N$ . From (28), we may write:

$$\|Y\|^{-1} \leq \frac{\|\hat{U}\|}{\|Y\hat{U}\|} \leq C, \tag{29}$$

Similarly, for the pseudoinverse  $Y^\dagger$  of  $Y$ , we can write:

$$\|Y^\dagger\| = \sup_{v \neq 0} \frac{\|Y^\dagger v\|}{\|v\|}. \tag{30}$$

Thus, we have:

$$\|Y^\dagger\| \geq \sup_{v=Y\hat{U} \neq 0} \frac{\|Y^\dagger Y\hat{U}\|}{\|Y\hat{U}\|} = \sup_{\hat{U} \neq 0} \frac{\|\hat{U}\|}{\|Y\hat{U}\|} = C. \tag{31}$$

We can see that Equations (29) and (31) confirm the bounds for the stability constant  $C$ . Calculating the pseudoinverse for approximating the system in Equation (27) numerically can be difficult computationally, but it ensures the stability. MATLAB's function `condest` can be used to estimate  $\|Y^{-1}\|_\infty$  in the case of square systems; thus, we have:

$$C = \frac{\text{condest}(Y')}{\|Y\|_\infty}. \tag{32}$$

**6. Numerical Results and Discussion**

The proposed Laplace transform based local meshless method is tested on 2D linear multi-term FPIDEs. In our numerical experiments, we utilized the multiquadric (MQ) radial kernel defined by  $\phi(r, \epsilon) = \sqrt{1 + (\epsilon r)^2}$ . For the optimal shape parameter, the uncertainty principle due to [53]

(e.g., in RBF methods, we cannot have both good accuracy and good conditioning at the same time) is utilized. We performed our experiments in MATLAB R2019a on a Windows 10(64 bit) PC equipped with an Intel(R) Core(TM) i5-3317U CPU @ 1.70 GHz and with 4 GB of RAM. We chose  $L = T = 1$ , and  $d_\rho = 1$ , for  $\rho = 1, 2, 3, \dots, m$ . Let  $U(\zeta, \tau)$  be the exact solution and  $U_k(\zeta, \tau)$  be the numerical solution. To validate the theoretical results, we used the  $L_\infty$  error defined as:

$$L_\infty = \|U(\zeta_i, \tau) - U_k(\zeta_i, \tau)\|_\infty = \max_{1 \leq i \leq N} (U(\zeta_i, \tau) - U_k(\zeta_i, \tau)).$$

In our numerical experiments, we consider the problem (1) with initial condition  $\Theta = 0$ , and the inhomogeneous term is given as:

$$f(x, y, \tau) = \Gamma\left(\frac{9}{5}\right) \left( \frac{\tau^{\frac{4}{5}-\gamma_1}}{\Gamma(\frac{9}{5}-\gamma_1)} + \frac{\tau^{\frac{4}{5}-\gamma_2}}{\Gamma(\frac{9}{5}-\gamma_2)} + \frac{2\pi^2\tau^{\frac{4}{5}+\alpha}}{\Gamma(\frac{9}{5}+\alpha)} \right) \sin(\pi x) \sin(\pi y).$$

The problem is solved with two types of boundary conditions, the Dirichlet boundary conditions generated from the exact solution given by:

$$U(x, y, \tau) = \tau^{\frac{4}{5}} \sin(\pi x) \sin(\pi y),$$

and the Robin boundary conditions given as:

$$U(x, y, \tau) + \nabla U(x, y, \tau) \cdot \vec{n} = \mathcal{G}(x, y, \tau), \quad x, y \in \partial\Omega, \quad \tau \in [0, 1].$$

We solve the problem in the square domain, nut-shaped domain, and L-shaped domain.

### 6.1. Square Domain

In the first test, the problem is solved in square domain  $[0, 1]^2$  with Dirichlet boundary conditions. The domain is discretized with regularly distributed nodes, as shown in the Figure 1. Then, the proposed scheme is applied to the 2D multi-term FPIDE. The exact and approximate solutions of the problem are presented in Figure 2a,b. The computational results obtained for various points  $N \in \Omega$ ,  $n \in \Omega_i$ , and quadrature points  $M$  along the contour  $\Gamma$  are given in Table 1. The  $L_\infty$  error, shape parameter  $\varepsilon$ , error estimate, condition number  $\kappa$ , and the computational time (CPU (s)) are shown in Table 1. The obtained results ensure the efficiency and stability of the method.

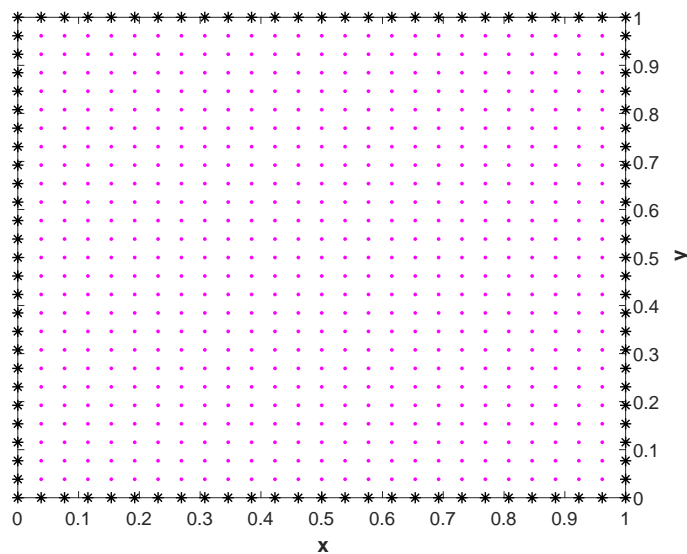
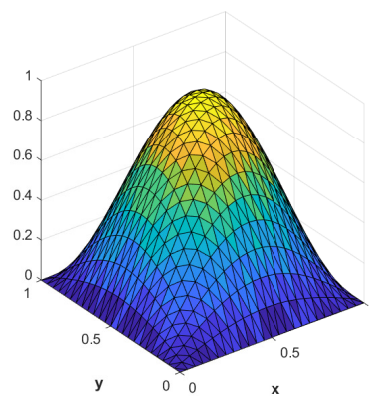


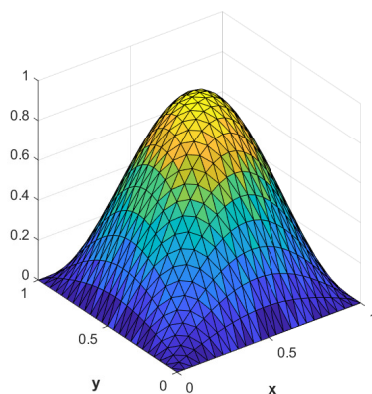
Figure 1. Node distribution in the square domain.

**Table 1.** Numerical results for the fractional partial integro-differential equations (FPIDEs) in the square domain.

	$N$	$n$	$M$	$L_\infty$ Error	Error Estimate	$\varepsilon$	$\kappa$	CPU(s)
$\alpha = 0.25$ $\gamma_1 = 0.15$ $\gamma_2 = 0.3$	1024	73	10	$1.90 \times 10^{-3}$	$1.26 \times 10^{-6}$	4.9	$1.54 \times 10^{12}$	7.395020
			12	$1.00 \times 10^{-3}$	$8.37 \times 10^{-8}$	4.9	$1.54 \times 10^{12}$	7.022358
			14	$9.94 \times 10^{-4}$	$5.53 \times 10^{-9}$	4.9	$1.54 \times 10^{12}$	7.249688
			16	$9.91 \times 10^{-4}$	$3.66 \times 10^{-10}$	4.9	$1.54 \times 10^{12}$	7.789044
			18	$9.91 \times 10^{-4}$	$2.42 \times 10^{-11}$	4.9	$1.54 \times 10^{12}$	8.160190
$\alpha = 0.5$ $\gamma_1 = 0.45$ $\gamma_2 = 0.55$			30	$2.20 \times 10^{-3}$	$1.60 \times 10^{-12}$	3.3	$1.40 \times 10^{12}$	6.398152
			40	$3.70 \times 10^{-3}$	$1.60 \times 10^{-12}$	4.0	$1.69 \times 10^{12}$	6.328329
			50	$2.0 \times 10^{-3}$	$1.60 \times 10^{-12}$	4.4	$1.56 \times 10^{12}$	7.150031
			60	$1.60 \times 10^{-3}$	$1.60 \times 10^{-12}$	4.7	$1.31 \times 10^{12}$	7.898109
			70	$1.60 \times 10^{-3}$	$1.60 \times 10^{-12}$	4.8	$2.10 \times 10^{12}$	8.372011
$\alpha = 0.75$ $\gamma_1 = 0.65$ $\gamma_2 = 0.75$	729	74	22	$1.10 \times 10^{-3}$	$1.05 \times 10^{-13}$	4.1	$1.64 \times 10^{12}$	5.758024
				$9.04 \times 10^{-4}$	$1.05 \times 10^{-13}$	4.5	$1.16 \times 10^{12}$	6.988687
				$8.75 \times 10^{-4}$	$1.05 \times 10^{-13}$	4.8	$1.26 \times 10^{12}$	10.074941
				$1.70 \times 10^{-3}$	$1.05 \times 10^{-13}$	5.1	$1.35 \times 10^{12}$	10.822728
				$8.47 \times 10^{-4}$	$1.05 \times 10^{-13}$	5.4	$1.44 \times 10^{12}$	13.236204
[40]				$7.16 \times 10^{-4}$				



(a)



(b)

**Figure 2.** (a) The exact solution in the square domain; (b) the numerical solution in the square domain.

6.2. Nut-Shaped Domain

In the second test, the problem is solved in the nut-shaped domain with Dirichlet boundary conditions. The domain is discretized with regularly distributed nodes, as shown in the Figure 3a. Then, the proposed scheme is applied to the 2D multi-term FPIDE. The exact and the numerical solutions of the problem are presented in Figure 3b. The computational results obtained for various points  $N \in \Omega$ ,  $n \in \Omega_i$ , and quadrature points  $M$  along the contour  $\Gamma$  are shown in Table 2. The  $L_\infty$  error, shape parameter  $\varepsilon$ , error estimate, condition number  $\kappa$ , and the computational time (CPU (s)) are shown in Table 2. The obtained results ensure the efficiency of the proposed method for problems defined in irregular domains.

Table 2. Numerical results for the FPIDEs in nut-shaped domain.

	$N$	$n$	$M$	$L_\infty$ Error	Error Estimate	$\varepsilon$	$\kappa$	CPU (s)
$\alpha = 0.25$	1024	76	10	$1.30 \times 10^{-3}$	$1.26 \times 10^{-6}$	4.9	$1.59 \times 10^{13}$	6.665154
$\gamma_1 = 0.15$			12	$2.71 \times 10^{-4}$	$8.37 \times 10^{-8}$	4.9	$1.59 \times 10^{13}$	7.059290
$\gamma_2 = 0.30$			14	$2.68 \times 10^{-4}$	$5.53 \times 10^{-9}$	4.9	$1.59 \times 10^{13}$	7.597790
			16	$2.69 \times 10^{-4}$	$3.66 \times 10^{-10}$	4.9	$1.59 \times 10^{13}$	8.066648
			18	$2.69 \times 10^{-4}$	$2.42 \times 10^{-11}$	4.9	$1.59 \times 10^{13}$	8.368624
$\alpha = 0.5$		30	20	$1.13 \times 10^{-2}$	$1.60 \times 10^{-12}$	3.2	$8.99 \times 10^{13}$	6.499886
$\alpha = 0.55$		40		$1.90 \times 10^{-3}$	$1.60 \times 10^{-12}$	3.8	$5.33 \times 10^{13}$	7.088308
$\alpha = 0.65$		50		$1.30 \times 10^{-3}$	$1.60 \times 10^{-12}$	4.3	$2.31 \times 10^{13}$	6.949834
		60		$1.70 \times 10^{-3}$	$1.60 \times 10^{-12}$	4.6	$1.68 \times 10^{13}$	7.556786
		74		$7.44 \times 10^{-4}$	$1.60 \times 10^{-12}$	4.9	$1.24 \times 10^{13}$	9.184561
$\alpha = 0.75$	973	75	22	$5.37 \times 10^{-4}$	$1.05 \times 10^{-13}$	5.0	$1.09 \times 10^{12}$	8.624205
$\gamma_1 = 0.75$	983			$2.48 \times 10^{-4}$	$1.05 \times 10^{-13}$	4.9	$1.76 \times 10^{12}$	9.407931
$\gamma_2 = 0.90$	993			$5.54 \times 10^{-4}$	$1.05 \times 10^{-13}$	5.0	$2.12 \times 10^{12}$	9.242420
	1003			$5.62 \times 10^{-4}$	$1.05 \times 10^{-13}$	4.9	$5.40 \times 10^{12}$	9.108576
	1013			$5.39 \times 10^{-4}$	$1.05 \times 10^{-13}$	4.9	$1.21 \times 10^{13}$	9.380810
[40]				$7.16 \times 10^{-4}$				

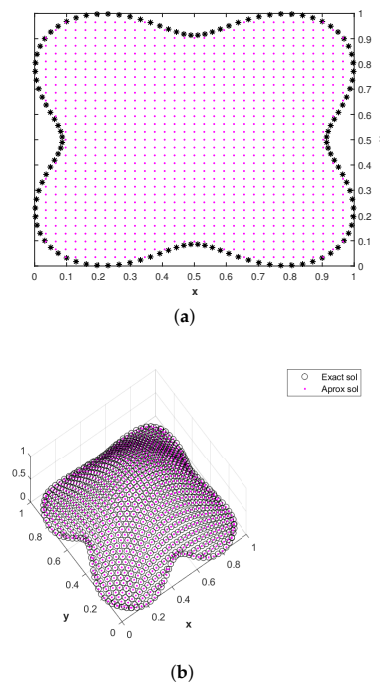


Figure 3. (a) Node distribution in the nut-shaped domain; (b) the exact and numerical solutions in the nut-shaped domain.

6.3. L-Shaped Domain

In the third test, the problem is solved in the L-shaped domain with Dirichlet and Robin boundary conditions. The domain is discretized with regularly distributed nodes, as shown in the Figure 4a. Then, the proposed method is applied to the 2D multi-term FPIDE. The exact and the numerical solutions of the problem are presented in Figure 4b. The computational results obtained for various points  $N \in \Omega$ ,  $n \in \Omega_i$ , and quadrature points  $M$  along the contour  $\Gamma$  with Dirichlet boundary conditions are shown in Table 3. The  $L_\infty$  error, shape parameter  $\varepsilon$ , error estimate, condition number  $\kappa$ , and the computational time (CPU (s)) are shown in Table 3. Figure 5 shows the absolute error obtained using Robin boundary conditions. The obtained results ensure the efficiency of the proposed method for problems defined in irregular domains.

Table 3. Numerical results for the FPIDEs in the L-shaped domain.

	$N$	$n$	$M$	$L_\infty$ Error	Error Estimate	$\varepsilon$	$\kappa$	CPU (s)
$\alpha = 0.25$ $\gamma_1 = 0.15$ $\gamma_2 = 0.30$	1045	75	10	$2.00 \times 10^{-3}$	$1.26 \times 10^{-6}$	5.4	$4.22 \times 10^{12}$	7.879603
			12	$9.70 \times 10^{-4}$	$8.37 \times 10^{-8}$	5.4	$4.22 \times 10^{12}$	8.472794
			14	$9.07 \times 10^{-4}$	$5.53 \times 10^{-9}$	5.4	$4.22 \times 10^{12}$	8.961569
			16	$9.03 \times 10^{-4}$	$3.66 \times 10^{-10}$	5.4	$4.22 \times 10^{12}$	9.776831
			18	$9.02 \times 10^{-4}$	$2.42 \times 10^{-11}$	5.4	$4.22 \times 10^{12}$	9.703955
$\alpha = 0.5$ $\gamma_1 = 0.45$ $\gamma_1 = 0.55$	736	73	20	$1.20 \times 10^{-3}$	$1.60 \times 10^{-12}$	3.4	$6.85 \times 10^{12}$	6.230811
			40	$1.70 \times 10^{-3}$	$1.60 \times 10^{-12}$	4.2	$8.39 \times 10^{12}$	7.051659
			50	$7.94 \times 10^{-4}$	$1.60 \times 10^{-12}$	4.8	$4.53 \times 10^{12}$	7.786541
			60	$8.99 \times 10^{-4}$	$1.60 \times 10^{-12}$	5.2	$3.21 \times 10^{12}$	8.323130
			72	$7.80 \times 10^{-4}$	$1.60 \times 10^{-12}$	5.4	$3.98 \times 10^{12}$	9.694111
$\alpha = 0.75$ $\gamma_1 = 0.75$ $\gamma_1 = 0.85$	1045	73	22	$7.68 \times 10^{-4}$	$1.05 \times 10^{-13}$	4.5	$4.06 \times 10^{12}$	5.941242
			833	$8.30 \times 10^{-4}$	$1.05 \times 10^{-13}$	4.8	$4.06 \times 10^{12}$	7.343621
			936	$6.45 \times 10^{-4}$	$1.05 \times 10^{-13}$	5.1	$4.06 \times 10^{12}$	8.402310
			1045	$7.49 \times 10^{-4}$	$1.05 \times 10^{-13}$	5.4	$4.06 \times 10^{12}$	10.279795
[40]			$7.16 \times 10^{-4}$					

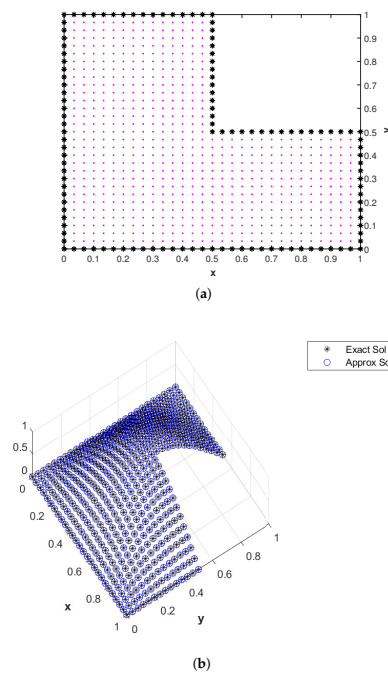
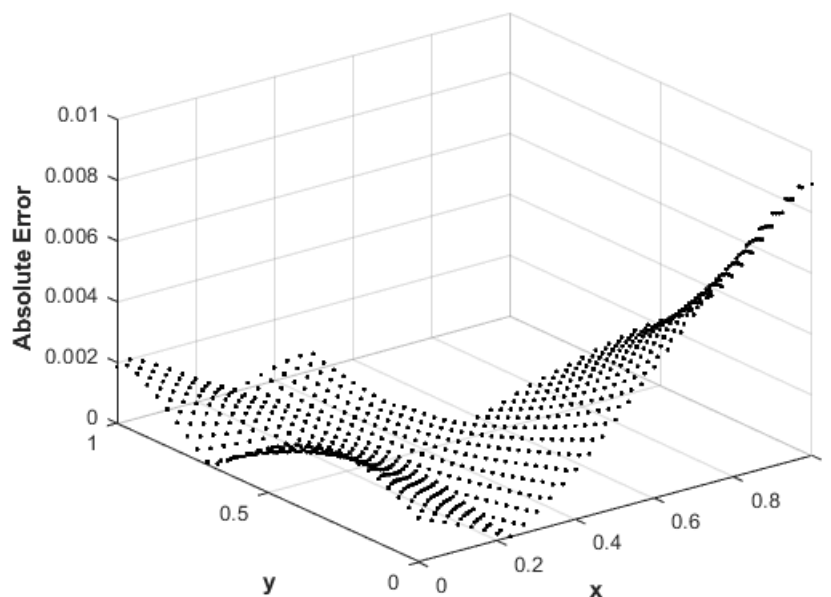


Figure 4. (a) Nodes in the L-shaped domain; (b) the exact and numerical solutions in the L-shaped domain.



**Figure 5.** Absolute error using Robin boundary conditions in the L-shaped domain, with  $\alpha = 0.5$ ,  $\gamma_1 = 0.75$ ,  $\gamma_2 = 0.95$ ,  $N = 736$ ,  $n = 73$ , and  $M = 20$ .

## 7. Conclusions

We successfully coupled the Laplace transform and localized meshless method for the approximation of the solution of the multi-term 2D FPIDE. The time stepping procedure was avoided via the Laplace transform, and the issues arising due to dense differentiation matrices were resolved via the localized meshless method. For the contour integration, we utilized the recently introduced improved Talbot's contour. The convergence and stability of the method were discussed. To validate the numerical scheme and check its efficiency, the numerical experiments were carried out in the square, nut-shaped, and L-shaped domains. From the results obtained, it was observed that the proposed numerical scheme is efficient and has better accuracy compared to other available work. It was observed that the improved Talbot's method is computationally more useful than other available methods. The results led us to the conclusion that the proposed method is capable of solving FPIDEs without time instability in less computation time.

**Author Contributions:** Conceptualization, K. and Z.S.; Data curation, Z.S.; Funding acquisition, Z.S. and P.K.; Investigation, K. and Z.S.; Methodology, K., Z.S. and P.K.; Project administration, Z.S. and P.K.; Software, K. and N.A.A.; Supervision, Z.S.; Validation, Z.S., P.K. and N.A.A.; Visualization, N.A.A.; Writing—original draft, K.; Writing—review & editing, P.K. and N.A.A. All authors have read and agreed to the published version of the manuscript.

**Funding:** This research received no external funding.

**Acknowledgments:** The authors acknowledge the financial support provided by the Center of Excellence in Theoretical and Computational Science (TaCS-CoE), KMUTT.

**Conflicts of Interest:** The authors declare no conflict of interest.

## References

1. Renardy, M. Mathematical analysis of viscoelastic flows. *Ann. Rev. Fluid Mech.* **1989**, *21*, 21–36. [[CrossRef](#)]
2. Al-Smadi, M.; Arqub, O.A. Computational algorithm for solving Fredholm time-fractional partial integro-differential equations of Dirichlet functions type with error estimates. *Appl. Math. Comput.* **2019**, *342*, 280–294.
3. Arshed, S. B-spline solution of fractional integro partial differential equation with a weakly singular kernel. *Numer. Methods Partial Differ. Equ.* **2017**, *33*, 1565–1581. [[CrossRef](#)]

4. Arqub, O.A.; Al-Smadi, M. Numerical algorithm for solving time-fractional partial integro-differential equations subject to initial and Dirichlet boundary conditions. *Numer. Methods Partial Differ. Equ.* **2018**, *34*, 1577–1597. [[CrossRef](#)]
5. Tang, T. A finite difference scheme for partial integro-differential equations with a weakly singular kernel. *Appl. Numer. Math.* **1993**, *11*, 309–319. [[CrossRef](#)]
6. Long, W.; Xu, D.; Zeng, X. Quasi wavelet based numerical method for a class of partial integro-differential equation. *Appl. Math. Comput.* **2012**, *218*, 11842–11850. [[CrossRef](#)]
7. Chen, C.; Thome, V.; Wahlbin, L.B. Finite element approximation of a parabolic integro-differential equation with a weakly singular kernel. *Math. Comput.* **1992**, *58*, 587–602. [[CrossRef](#)]
8. Xu, D. On the discretization in time for a parabolic integro-differential equation with a weakly singular kernel I: Smooth initial data. *Appl. Math. Comput.* **1993**, *58*, 1–27.
9. Wulan, L.; Xu, D. Finite central difference/finite element approximations for parabolic integro-differential equations. *Computing* **2010**, *90*, 89–111.
10. EL-Asyed, A.M.A.; Soliman, A.F.; El-Azab, M.S. On the numerical solution of partial integro-differential equations. *Math. Sci. Lett.* **2012**, *1*, 71–80.
11. Fairweather, G. Spline collocation methods for a class of hyperbolic partial integro-differential equations. *SIAM J. Numer. Anal.* **1994**, *31*, 444–460. [[CrossRef](#)]
12. Siddiqi, S.S.; Arshed, S. Cubic B-spline for the Numerical Solution of Parabolic Integro-differential Equation with a Weakly Singular Kernel. *Res. J. Appl. Sci. Eng. Technol.* **2014**, *7*, 2065–2073. [[CrossRef](#)]
13. Huang, Y.Q. Time discretization scheme for an integro-differential equation of parabolic type. *J. Comput. Math.* **1994**, *12*, 259–263.
14. Hu, S.; Qiu, W.; Chen, H. A backward Euler difference scheme for the integro-differential equations with the multi-term kernels. *Int. J. Comput. Math.* **2020**, *97*, 1254–1267. [[CrossRef](#)]
15. Kılıçman, A.; Ahmood, W.A. Solving multi-dimensional fractional integro-differential equations with the initial and boundary conditions by using multi-dimensional Laplace Transform method. *Tbilisi Math. J.* **2017**, *10*, 105–115. [[CrossRef](#)]
16. Gu, X.M.; Wu, S.L. A parallel-in-time iterative algorithm for Volterra partial integral-differential problems with weakly singular kernel. *J. Comput. Phys.* **2020**, *417*, 109576. [[CrossRef](#)]
17. Saadatmandi, A.; Khani, A.; Azizi, M.R. A sinc-Gauss-Jacobi collocation method for solving Volterra's population growth model with fractional order. *Tbilisi Math. J.* **2018**, *11*, 123–137. [[CrossRef](#)]
18. Moradi, L.; Mohammadi, F.; Conte, D. A discrete orthogonal polynomials approach for coupled systems of nonlinear fractional order integro-differential equations. *Tbilisi Math. J.* **2019**, *12*, 21–38. [[CrossRef](#)]
19. Alsaedi, A.; Agarwal, R.P.; Ntouyas, S.K.; Ahmad, B. Fractional-Order Integro-Differential Multivalued Problems with Fixed and Nonlocal Anti-Periodic Boundary Conditions. *Mathematics* **2020**, *8*, 1774. [[CrossRef](#)]
20. Ahmad, B.; Broom, A.; Alsaedi, A.; Ntouyas, S.K. Nonlinear integro-differential equations involving mixed right and left fractional derivatives and integrals with nonlocal boundary data. *Mathematics* **2020**, *8*, 336. [[CrossRef](#)]
21. Amin, R.; Nazir, S.; García-Magariño, I. A Collocation Method for Numerical Solution of Nonlinear Delay Integro-Differential Equations for Wireless Sensor Network and Internet of Things. *Sensors* **2020**, *20*, 1962. [[CrossRef](#)]
22. Nemati, S.; Torres, D.F. Application of Bernoulli Polynomials for Solving Variable-Order Fractional Optimal Control-Affine Problems. *Axioms* **2020**, *9*, 114. [[CrossRef](#)]
23. Holhos, A.; Rosca, D. Orthonormal wavelet bases on the 3D ball via volume preserving map from the regular octahedron. *arXiv* **2019**, arXiv:1910.08067.
24. Jäntschi, L. The eigenproblem translated for alignment of molecules. *Symmetry* **2019**, *11*, 1027. [[CrossRef](#)]
25. Bazgir, H.; Ghazanfari, B. Existence of Solutions for Fractional Integro-Differential Equations with Non-Local Boundary Conditions. *Math. Comput. Appl.* **2018**, *23*, 36. [[CrossRef](#)]
26. Georgieva, A. Double Fuzzy Sumudu Transform to Solve Partial Volterra Fuzzy Integro-Differential Equations. *Mathematics* **2020**, *8*, 692. [[CrossRef](#)]
27. Biazar, J.; Asadi, M.A. FD-RBF for partial integro-differential equations with a weakly singular kernel. *Appl. Comput. Math.* **2015**, *4*, 445–451. [[CrossRef](#)]

28. Ali, G.; Gómez-Aguilar, J.F. Approximation of partial integro differential equations with a weakly singular kernel using local meshless method. *Alex. Eng. J.* **2020**, *59*, 2091–2100. [[CrossRef](#)]
29. Aslefallah, M.; Shivanian, E. A nonlinear partial integro-differential equation arising in population dynamic via radial basis functions and theta-method. *J. Math. Comput. Sci.* **2014**, *13*, 14–25. [[CrossRef](#)]
30. Safinejad, M.; Moghaddam, M.M. A local meshless RBF method for solving fractional integro-differential equations with optimal shape parameters. *Ital. J. Pure Appl. Math.* **2019**, *41*, 382.
31. Fu, Z.J.; Chen, W.; Yang, H.T. Boundary particle method for Laplace transformed time fractional diffusion equations. *J. Comput. Phys.* **2013**, *235*, 52–66. [[CrossRef](#)]
32. Davies, A.J.; Crann, D.; Mushtaq, J. A parallel implementation of the Laplace transform BEM. *WIT Trans. Model. Simul.* **1970**, *14*. [[CrossRef](#)]
33. Gia, Q.T.L.; Mclean, W. Solving the heat equation on the unit sphere via Laplace transforms and radial basis functions. *Adv. Comput. Math.* **2014**, *40*, 353–375. [[CrossRef](#)]
34. McLean, W.; Thomee, V. Numerical solution via Laplace transforms of a fractional order evolution equation. *J. Integral Equ. Appl.* **2010**, *22*, 57–94. [[CrossRef](#)]
35. Fernandez, M.L.; Palencia, C. On the numerical inversion of the Laplace transform of certain holomorphic mappings. *Appl. Numer. Math.* **2004**, *51*, 289–303. [[CrossRef](#)]
36. Jacobs, B.A. High-order compact finite difference and Laplace transform method for the solution of time fractional heat equations with Dirichlet and Neumann boundary conditions. *Numer. Methods Partial Differ. Equ.* **2016**, *32*, 1184–1199. [[CrossRef](#)]
37. Li, X.; Kamran; Haq, A.; Zhang, X. Numerical solution of the linear time fractional Klein-Gordon equation using transform based localized RBF method and quadrature. *AIMS Math.* **2020**, *5*, 5287–5308. [[CrossRef](#)]
38. Uddin, M.; Ali, A. A localized transform-based meshless method for solving time fractional wave-diffusion equation. *Eng. Anal. Bound. Elem.* **2018**, *92*, 108–113. [[CrossRef](#)]
39. Li, J.; Dai, L.; Nazeer, W. Numerical solution of multi-term time fractional wave diffusion equation using transform based local meshless method and quadrature. *AIMS Math.* **2020**, *5*, 5813–5838. [[CrossRef](#)]
40. Zhou, J.; Xu, D. Alternating direction implicit difference scheme for the multi-term time-fractional integro-differential equation with a weakly singular kernel. *Comput. Math. Appl.* **2020**, *79*, 244–255. [[CrossRef](#)]
41. Oldham, K.B.; Spanier, J. *The Fractional Calculus Theory and Applications of Differentiation and Integration to Arbitrary Order*; Academic Press: New York, NY, USA; London, UK, 1974; Volume 111.
42. Podlubny, I. Fractional Differential Equations. In *Mathematics in Science and Engineering*; Elsevier: Amsterdam, The Netherlands, 1999; Volume 198.
43. Popolizio, M. Numerical solution of multiterm fractional differential equations using the matrix Mittag-Leffler functions. *Mathematics* **2018**, *6*, 7. [[CrossRef](#)]
44. Schiessel, H.; Metzler, R.; Blumen, A.; Nonnenmacher, T.F. Generalized viscoelastic models: Their fractional equations with solutions. *J. Phys. A Math. Gen.* **1995**, *28*, 6567. [[CrossRef](#)]
45. Torvik, P.J.; Bagley, R.L. On the appearance of the fractional derivative in the behavior of real materials. *J. Appl. Mech.* **1984**, *51*, 294–298. [[CrossRef](#)]
46. Qin, S.; Liu, F.; Turner, I.; Vegh, V.; Yu, Q.; Yang, Q. Multi-term time-fractional Bloch equations and application in magnetic resonance imaging. *J. Comput. Appl. Math.* **2017**, *319*, 308–319. [[CrossRef](#)]
47. Diethelm, K. *The Analysis of Fractional Differential Equations: An Application-Oriented Exposition Using Differential Operators of Caputo Type*; Springer Science & Business Media: Berlin, Germany, 2010.
48. Šarler, B.; Vertnik, R. Meshfree explicit local radial basis function collocation method for diffusion problems. *Comput. Math. Appl.* **2006**, *51*, 1269–1282. [[CrossRef](#)]
49. Talbot, A. The accurate numerical inversion of Laplace transform. *J. Inst. Math. Appl.* **1979**, *23*, 97–120. [[CrossRef](#)]
50. Dingfelder, B.; Weideman, J.A.C. An improved Talbot method for numerical Laplace transform inversion. *Numer. Algorithms* **2015**, *68*, 167–183. [[CrossRef](#)]
51. Weideman, J.A.C. Optimizing Talbot's contours for the inversion of the Laplace transform. *SIAM J. Numer. Anal.* **2006**, *44*, 2342–2362. [[CrossRef](#)]
52. Sarra, S.A.; Kansa, E.J. Multiquadric radial basis function approximation methods for the numerical solution of partial differential equations. *Adv. Comput. Mech.* **2009**, *2*.

53. Schaback, R. Error estimates and condition numbers for radial basis function interpolation. *Adv. Comput. Math.* **1995**, *3*, 251–264. [[CrossRef](#)]

**Publisher’s Note:** MDPI stays neutral with regard to jurisdictional claims in published maps and institutional affiliations.



© 2020 by the authors. Licensee MDPI, Basel, Switzerland. This article is an open access article distributed under the terms and conditions of the Creative Commons Attribution (CC BY) license (<http://creativecommons.org/licenses/by/4.0/>).